

Testing general relativity with the stellar-mass black hole in LMC X-1 using the continuum-fitting method

Ashutosh Tripathi,¹ Menglei Zhou,¹ Askar B. Abdikamalov,¹ Dimitry Ayzenberg,¹ Cosimo Bambi,^{1,*} Lijun Gou,^{2,3} Victoria Grinberg,⁴ Honghui Liu,¹ and James F. Steiner⁵

¹*Center for Field Theory and Particle Physics and Department of Physics, Fudan University, 200438 Shanghai, China*

²*Key Laboratory for Computational Astrophysics, National Astronomical Observatories, Chinese Academy of Sciences, 100012 Beijing, China*

³*School of Astronomy and Space Science, University of Chinese Academy of Sciences, 100049 Beijing, China*

⁴*Institut für Astronomie und Astrophysik (IAAT),*

Eberhard-Karls Universität Tübingen, 72076 Tübingen, Germany

⁵*Harvard-Smithsonian Center for Astrophysics, Cambridge, MA 02138, United States*

The iron line and the continuum-fitting methods are currently the two leading techniques for measuring black hole spins with electromagnetic radiation. They can be naturally extended for probing the spacetime geometry around black holes and testing general relativity in the strong field regime. In the past couple of years, there has been significant work to use the iron line method to test the nature of black holes. In this Letter, we use the continuum-fitting method and we show its capability of constraining the spacetime geometry around black holes by analyzing 17 *RXTE* data of the X-ray binary LMC X-1.

Einstein's theory of general relativity was proposed over a century ago and has successfully passed a large number of observational tests, mainly in the weak field regime [1]. Thanks to new observational facilities, tests of general relativity in the strong field regime are a hot topic nowadays. Astrophysical black holes are ideal laboratories for testing strong gravity. The spacetime geometry around these objects is thought to be well approximated by the Kerr solution [2, 3], as deviations induced by a non-vanishing electric charge or by the presence of accretion disks or nearby stars is usually completely negligible [4–6]. On the other hand, macroscopic deviations from the Kerr geometry are predicted in models with exotic fields [7], in a number of modified theories of gravity [8], or as a result of large quantum gravity effects near the black hole event horizon [9–11].

Black holes can be tested either with electromagnetic or gravitational wave techniques, and the two approaches are complementary. Electromagnetic tests [12], strictly speaking, are more suitable to probe the couplings between the gravity and the matter sectors (geodesic motion of particles and non-gravitational physics in presence of gravity). Gravitational wave tests [13] can probe better the gravity sector itself (Einstein's Equations). It may be possible that new physics only shows up in one of the two spectra and not in the other one. When the two approaches can be compared to test the Kerr metric around black holes, they seem to provide similar constraints [14].

The two leading electromagnetic techniques for measuring black hole spins under the assumption of the Kerr metric are X-ray reflection spectroscopy (or analysis of the iron line) [15, 16] and the continuum-fitting method (or analysis of the thermal spectrum) [17, 18]. Both techniques can be naturally extended to test the Kerr black

hole hypothesis [19–23]. In the past few years, there has been significant work to test black holes using X-ray reflection spectroscopy and there are now a number of published results on observational constraints using data from *XMM-Newton*, *Suzaku*, and *NuSTAR* data [24–28]. In this Letter, we start testing the Kerr metric using the continuum-fitting method. We employ our new model NKBB [29] and we analyze 17 *RXTE* observations of the stellar-mass black hole in LMC X-1 to constrain possible deviations from the Kerr solution.

The continuum-fitting method is the analysis of the thermal spectrum of a geometrically thin and optically thick accretion disk around a black hole [17]. Geometrically thin accretion disks are normally described by the Novikov-Thorne model [30, 31], which is the relativistic generalization of the Shakura-Sunyaev model [32]. The disk is assumed to be on the equatorial plane, perpendicular to the black hole spin, and the inner edge of the disk is set at the innermost stable circular orbit (ISCO). From the conservation of mass, energy, and angular momentum, we infer the time averaged radial structure of the disk. In the Kerr spacetime, the thermal spectrum of the disk turns out to depend only on five parameters: black hole distance D , inclination angle of the disk with respect to the line of sight of the observer i , black hole mass M , black hole spin parameter a_* , and mass accretion rate \dot{M} . Since the spectrum is degenerate with respect to these five parameters, spin measurements require independent estimates of D , i , and M , and the fit can provide the spin parameter a_* and the mass accretion rate \dot{M} [17, 18].

NKBB follows the so called bottom-up approach. The thermal spectrum of the accretion disk is calculated in a parametric black hole spacetime, where possible deviations from the Kerr geometry are quantified by introducing *ad hoc* deformation parameters. The spirit behind this approach is to perform a null-experiment and check

* Corresponding author: bambi@fudan.edu.cn

whether astronomical data require that all deformation parameters vanish; that is, the Kerr metric is sufficient to model the data well. Among the many proposed parametric black hole spacetimes in literature, here we use the Johannsen metric [33], whose line element and basic properties are briefly reviewed in the Supplemental Material (SM). As a preliminary study to illustrate the constraining power of the continuum-fitting method to test the Kerr metric, we employ the simplest version of the Johannsen metric with only one deformation parameter, α_{13} .

LMC X-1 was discovered in 1969 as the first extragalactic X-ray binary [34, 35]. The system consists of a stellar-mass black hole and an O-giant companion star. The distance of the source, the black hole mass, and the inclination angle of the orbit, which are three key-quantities in the continuum-fitting method, have been estimated to be $D = 48.10 \pm 2.22$ kpc, $M = 10.91 \pm 1.54 M_{\odot}$, and $i = 36.38 \pm 2.02$ deg, respectively [36, 37]. LMC X-1 is characterized by a quite stable bolometric luminosity, which is about 16% of its Eddington luminosity L_{Edd} [37] and thus nicely meets the standard criterion required to use the continuum-fitting method: sources with an accretion luminosity in the range 5% to 30% L_{Edd} [18].

The measurement of the spin parameter of the black hole in LMC X-1 using the continuum-fitting method was presented in [37], and here we follow that study. There are 55 pointed observations of LMC X-1 with the Proportional Counter Array (PCA) onboard *RXTE* [38]. To use the continuum-fitting method, it is desirable to choose thermal dominant spectral data, which are defined by three conditions [39]: *i*) the flux of the thermal component accounts for more than 75% of the total 2-20 keV unabsorbed flux, *ii*) the root mean square (RMS) variability in the power density spectrum in the 0.1-10 Hz range is lower than 0.075, and *iii*) quasi-periodic oscillations (QPOs) are absent or very weak. Imposing these three conditions, we only have 3 observations, which are named “gold spectra” in [37] as they are supposed to be more suitable for the continuum-fitting method. Relaxing condition *i*), we have 14 more observations, which are named “silver spectra” in [37]¹. Additionally, we require that the accretion luminosity is in the range 5% to 30% in order to assure that the accretion disk is geometrically thin and the inner edge is at the ISCO [18], but this is always satisfied in the *RXTE* observations of LMC X-1.

The data reduction is described in SM. We fit each of the 17 observations with the XSPEC model [40]

$$\text{TBABS} \times (\text{SIMPL} \times \text{NKBB}) .$$

TBABS describes the Galactic absorption [41] and we freeze the hydrogen column density to $N_{\text{H}} = 4.6 \cdot 10^{21} \text{ cm}^{-2}$ [36]; however, its exact value does not matter

considering it is low and we are analyzing *RXTE* data. NKBB describes the thermal spectrum of the accretion disk [29]. The distance of the source D , the black hole mass M , and the inclination angle of the orbit i are frozen to 48.10 kpc, 10.91 M_{\odot} , and 36.38 deg, respectively; at this stage, we ignore their uncertainties. The hardening factor is frozen to 1.55 for all observations, which is the value found in [37]. We checked that its impact is weak and we get very similar results even if we use 1.45 or 1.65. The hardening factor varies with luminosity, but LMC X-1 varies modestly around 16% of its Eddington limit, which justifies the use of a fixed value. The spin parameter a_* and the mass accretion rate are always free parameters to be determined by the fit. The deformation parameter α_{13} is first set to zero (Kerr metric) in order to check if we can recover the results of Ref. [37], and then it is left free in order to measure possible deviations from the Kerr spacetime. SIMPL converts a fraction f_{SC} of thermal photons into a power-law-like spectrum with photon index Γ to describe the radiation from the corona [42], providing a superior description of the Comptonization at low energies as compared to a power-law. Since the data do not permit us to determine Γ , we freeze it to 2.5, as in [37]. Employing a different value for Γ has a marginal impact on the estimate of the other parameters [37]. In the end, the model has 3 free parameters (a_* , M , and f_{SC}) when we assume the Kerr metric and 4 (even α_{13}) otherwise.

The constraints on the spin parameter a_* and the deformation parameter α_{13} for every observation are shown in Fig. 1, while Tab. I in SM summarizes the best-fit values. Roughly speaking, the continuum fitting method measures the position of the inner edge of the disk, which is set at the ISCO in the Novikov-Thorne model and only depends on the spin parameter in the Kerr spacetime. This allows us to measure the black hole spin when we assume the Kerr metric. Relaxing the Kerr hypothesis, the situation is more complicated. As we can see from Fig. 1, there is a strong correlation between a_* and α_{13} . Now the ISCO is set by a_* and α_{13} (see [43] for more details), so it is difficult to constrain the values of a_* and α_{13} . If we combine all observations together², we obtain the constraints in Fig. 2 and the measurement of a_* and α_{13} is (90% confidence level for one relevant parameter)

$$a_* = 0.998_{-0.44} , \quad \alpha_{13} = 0.32_{-3.1}^{+0.04} . \quad (1)$$

In order to take the observational uncertainties of D , M , and i into account, we proceed as in Ref. [37] and we run Monte Carlo simulations assuming that the uncertainties in these parameters are normally and independently distributed. The result of 2,000 simulations is shown in Fig. 3. Contrary to the Kerr case, in which the uncertainties of D , M , and i provide the main contribution on the final uncertainty on a_* , in the non-Kerr case

¹ We note that in [37] there are 15 silver spectra, but here we ignore one of these observations because of a problem in the current version of the ftool RBNRMF.

² To combine all observations together, we take the average of the χ^2 at each grid-point in the (a_*, α_{13}) plane.

their impact is small and eventually subdominant with respect to the statistical uncertainty shown in Eq. (1). Our final measurement of a_* and α_{13} is thus given in Eq. (1).

This work was supported by the Innovation Program of the Shanghai Municipal Education Commission,

Grant No. 2019-01-07-00-07-E00035, and the National Natural Science Foundation of China (NSFC), Grant No. 11973019. A.T., C.B., V.G., H.L., and J.F.S. are members of the International Team 458 at the International Space Science Institute (ISSI), Bern, Switzerland, and acknowledge support from ISSI during the meetings in Bern.

-
- [1] C. M. Will, *Living Rev. Rel.* **17**, 4 (2014) [arXiv:1403.7377 [gr-qc]].
- [2] R. P. Kerr, *Phys. Rev. Lett.* **11**, 237 (1963).
- [3] B. Carter, *Phys. Rev. Lett.* **26**, 331 (1971).
- [4] C. Bambi, A. D. Dolgov and A. A. Petrov, *JCAP* **0909**, 013 (2009) [arXiv:0806.3440 [astro-ph]].
- [5] C. Bambi, D. Malafarina and N. Tsukamoto, *Phys. Rev. D* **89**, 127302 (2014) [arXiv:1406.2181 [gr-qc]].
- [6] C. Bambi, *Annalen Phys.* **530**, 1700430 (2018) [arXiv:1711.10256 [gr-qc]].
- [7] C. A. R. Herdeiro and E. Radu, *Phys. Rev. Lett.* **112**, 221101 (2014) [arXiv:1403.2757 [gr-qc]].
- [8] D. Ayzenberg and N. Yunes, *Phys. Rev. D* **90**, 044066 (2014) [Erratum: *Phys. Rev. D* **91**, 069905 (2015)] [arXiv:1405.2133 [gr-qc]].
- [9] G. Dvali and C. Gomez, *Fortsch. Phys.* **61**, 742 (2013) [arXiv:1112.3359 [hep-th]].
- [10] S. B. Giddings and D. Psaltis, *Phys. Rev. D* **97**, 084035 (2018) [arXiv:1606.07814 [astro-ph.HE]].
- [11] R. Carballo-Rubio, F. Di Filippo, S. Liberati and M. Visser, arXiv:1911.11200 [gr-qc].
- [12] C. Bambi, *Rev. Mod. Phys.* **89**, 025001 (2017) [arXiv:1509.03884 [gr-qc]].
- [13] K. Yagi and L. C. Stein, *Class. Quant. Grav.* **33**, 054001 (2016) [arXiv:1602.02413 [gr-qc]].
- [14] A. Cardenas-Avendano, S. Nampalliwar and N. Yunes, arXiv:1912.08062 [gr-qc].
- [15] L. W. Brenneman and C. S. Reynolds, *Astrophys. J.* **652**, 1028 (2006) [astro-ph/0608502].
- [16] C. S. Reynolds, *Space Sci. Rev.* **183**, 277 (2014) [arXiv:1302.3260 [astro-ph.HE]].
- [17] S. N. Zhang, W. Cui and W. Chen, *Astrophys. J.* **482**, L155 (1997) [astro-ph/9704072].
- [18] J. E. McClintock, R. Narayan and J. F. Steiner, *Space Sci. Rev.* **183**, 295 (2014) [arXiv:1303.1583 [astro-ph.HE]].
- [19] J. Schee and Z. Stuchlik, *Gen. Rel. Grav.* **41**, 1795 (2009) [arXiv:0812.3017 [astro-ph]].
- [20] C. Bambi, *Phys. Rev. D* **87**, 023007 (2013) [arXiv:1211.2513 [gr-qc]].
- [21] C. Bambi, A. Cardenas-Avendano, T. Dauser, J. A. Garcia and S. Nampalliwar, *Astrophys. J.* **842**, 76 (2017) [arXiv:1607.00596 [gr-qc]].
- [22] C. Bambi and E. Barausse, *Astrophys. J.* **731**, 121 (2011) [arXiv:1012.2007 [gr-qc]].
- [23] C. Bambi, *Astrophys. J.* **761**, 174 (2012) [arXiv:1210.5679 [gr-qc]].
- [24] Z. Cao, S. Nampalliwar, C. Bambi, T. Dauser and J. A. Garcia, *Phys. Rev. Lett.* **120**, 051101 (2018) [arXiv:1709.00219 [gr-qc]].
- [25] A. Tripathi, S. Nampalliwar, A. B. Abdikamalov, D. Ayzenberg, C. Bambi, T. Dauser, J. A. Garcia and A. Marinucci, *Astrophys. J.* **875**, 56 (2019) [arXiv:1811.08148 [gr-qc]].
- [26] A. Tripathi *et al.*, *Astrophys. J.* **874**, 135 (2019) [arXiv:1901.03064 [gr-qc]].
- [27] A. B. Abdikamalov, D. Ayzenberg, C. Bambi, T. Dauser, J. A. Garcia and S. Nampalliwar, *Astrophys. J.* **878**, 91 (2019) [arXiv:1902.09665 [gr-qc]].
- [28] Y. Zhang, A. B. Abdikamalov, D. Ayzenberg, C. Bambi and S. Nampalliwar, *Astrophys. J.* **884**, 147 (2019) [arXiv:1907.03084 [gr-qc]].
- [29] M. Zhou, A. B. Abdikamalov, D. Ayzenberg, C. Bambi, H. Liu and S. Nampalliwar, *Phys. Rev. D* **99**, 104031 (2019) [arXiv:1903.09782 [gr-qc]].
- [30] I. D. Novikov and K. S. Thorne, in *Black Holes*, eds. C. DeWitt and B. S. DeWitt (Gordon and Breach, New York, 1973), pp. 343-450.
- [31] D. N. Page and K. S. Thorne, *Astrophys. J.* **191**, 499 (1974).
- [32] N. I. Shakura and R. A. Sunyaev, *Astron. Astrophys.* **24**, 337 (1973).
- [33] T. Johannsen, *Phys. Rev. D* **88**, 044002 (2013) [arXiv:1501.02809 [gr-qc]].
- [34] H. Mark, R. Price, R. Rodrigues, F. D. Seward and C. D. Swift, *Astrophys. J.* **155**, L143 (1969).
- [35] R. E. Price, D. J. Groves, R. Rodrigues, F. D. Seward, C. D. Swift and A. Toor, *Astrophys. J.* **168**, L7 (1971).
- [36] J. A. Orosz *et al.*, *Astrophys. J.* **697**, 573 (2009) [arXiv:0810.3447 [astro-ph]].
- [37] L. Gou, J. E. McClintock, J. Liu, R. Narayan, J. F. Steiner, R. A. Remillard, J. A. Orosz and S. W. Davis, *Astrophys. J.* **701**, 1076 (2009) [arXiv:0901.0920 [astro-ph.HE]].
- [38] J. H. Swank, *Nucl. Phys. B Proc. Suppl.* **69**, 12 (1999).
- [39] R. A. Remillard and J. E. McClintock, *Ann. Rev. Astron. Astrophys.* **44**, 49 (2006) [astro-ph/0606352].
- [40] K. A. Arnaud, *Astronomical Data Analysis Software and Systems V*, **101**, 17 (1996).
- [41] J. Wilms, A. Allen and R. McCray, *Astrophys. J.* **542**, 914 (2000) [astro-ph/0008425].
- [42] J. F. Steiner, R. Narayan, J. E. McClintock and K. Ebisawa, *Publ. Astron. Soc. Pac.* **121**, 1279 (2009) [arXiv:0810.1758 [astro-ph]].
- [43] L. Kong, Z. Li and C. Bambi, *Astrophys. J.* **797**, 78 (2014) [arXiv:1405.1508 [gr-qc]].
- [44] A. Tripathi, S. Nampalliwar, A. B. Abdikamalov, D. Ayzenberg, J. Jiang and C. Bambi, *Phys. Rev. D* **98**, 023018 (2018) [arXiv:1804.10380 [gr-qc]].
- [45] J. A. Garcia, J. E. McClintock, J. F. Steiner, R. A. Remillard and V. Grinberg, *Astrophys. J.* **794**, 73 (2014) [arXiv:1408.3607 [astro-ph.HE]].
- [46] K. Jahoda, C. B. Markwardt, Y. Radeva, A. H. Rots, M. J. Stark, J. H. Swank, T. E. Strohmayer and

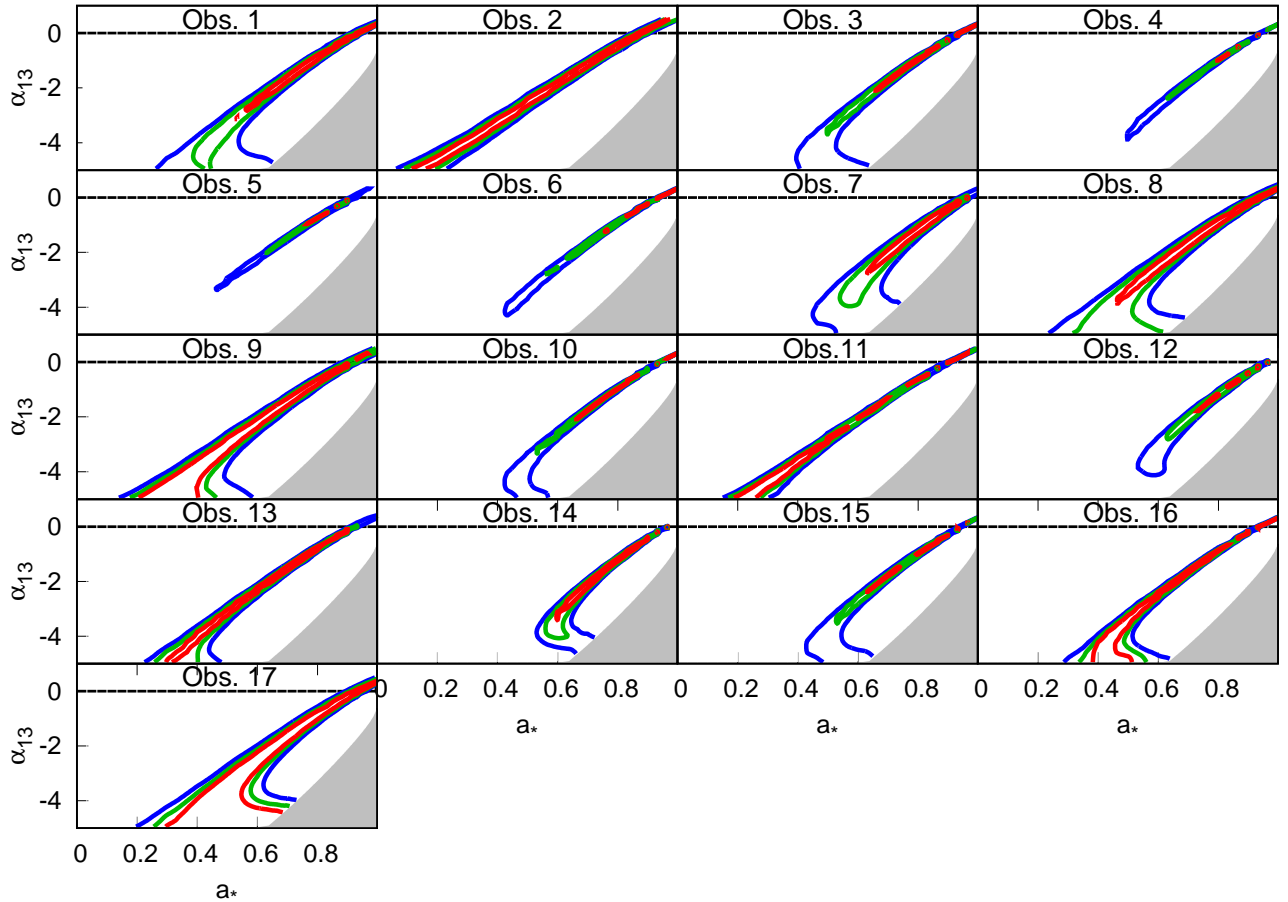


FIG. 1. Constraints on the spin parameter a_* and the deformation parameter α_{13} for observations 1-17. The red, green, and blue curves represent, respectively, the 68%, 90% and 99% confidence level curves for two relevant parameters ($\Delta\chi^2 = 2.30, 4.61, \text{ and } 9.21$, respectively). The gray region is ignored because it includes pathological spacetimes (see SM for more details).

SUPPLEMENTAL MATERIAL

Johannsen metric

The Johannsen metric is not a black hole solution from a specific theory of gravity but a parametric black hole metric in which possible deviations from the Kerr geometry are quantified by an infinite number of deformation parameters [33]. The Johannsen metric exactly reduces to the Kerr metric when all the deformation parameters vanish. It can thus be used to test the Kerr metric within the spirit of a null-experiment: we fit astronomical data of black holes to infer the values of the deformation parameters and check whether they vanish, as is required by the Kerr solution. If a possible deviation from the Kerr solution is found, the Johannsen metric is not suitable to measure the deviation from the Kerr geometry and it is necessary to use a different approach.

In its simplest form, which is the version employed in our work, the Johannsen metric has only one deformation parameter, named α_{13} (see [33] for the origin of this parameter). In Boyer-Lindquist coordinates, the line el-

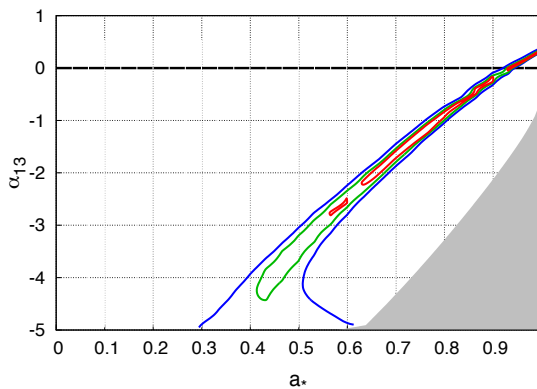


FIG. 2. As in Fig. 1 when we combine all observations together. See the text for more details.

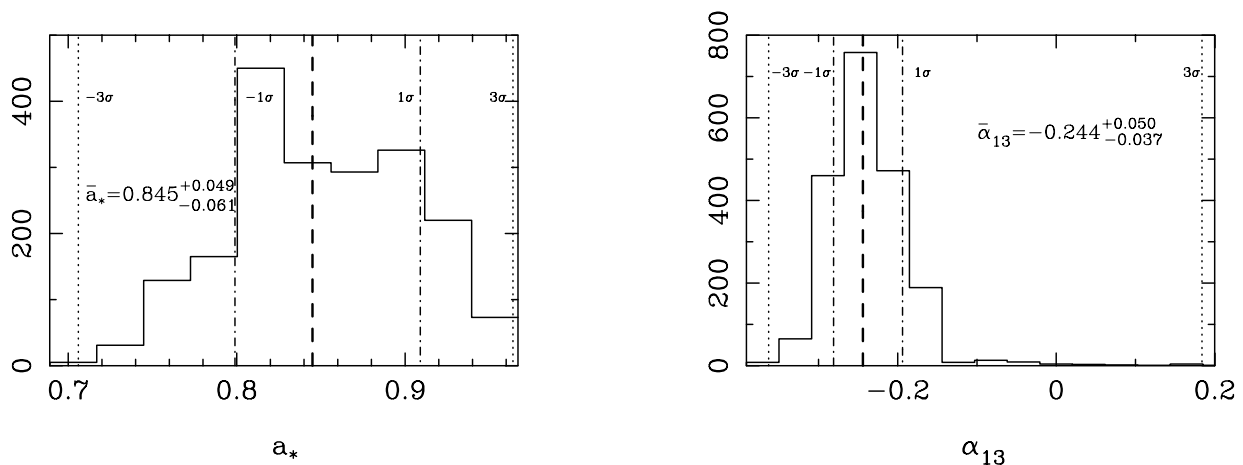


FIG. 3. Histograms of the spin parameter a_* (left panel) and of the deformation parameter α_{13} (right panel) for 2,000 sets of parameters (M, D, i) . The thick-dashed vertical lines mark the mean value of the fitting parameter, while the thin-dotted-dashed and thin-dotted vertical lines mark, respectively, the $1\text{-}\sigma$ and $3\text{-}\sigma$ limits. See the text for more details.

ement reads (we use units in which $G_N = c = 1$)

$$\begin{aligned}
 ds^2 = & -\frac{\Sigma(\Sigma - 2Mr)}{A^2} dt^2 + \frac{\Sigma}{\Delta} dr^2 + \Sigma d\theta^2 \\
 & + \frac{[(r^2 + a^2)^2(1 + \delta)^2 - a^2\Delta \sin^2\theta] \Sigma \sin^2\theta}{A^2} d\phi^2 \\
 & - \frac{2a[2Mr + \delta(r^2 + a^2)] \Sigma \sin^2\theta}{A^2} dt d\phi, \quad (2)
 \end{aligned}$$

where $a = a_*M$, $\Sigma = r^2 + a^2 \cos^2\theta$, $\Delta = r^2 - 2Mr + a^2$, and

$$A = \Sigma + \delta(r^2 + a^2), \quad \delta = \alpha_{13} \left(\frac{M}{r}\right)^3. \quad (3)$$

For $\alpha_{13} = 0$, we recover the Kerr metric. In order to have a regular exterior region, we have to impose $|a_*| \leq 1$ (as in the Kerr metric, for $|a_*| > 1$ there is no event horizon and the central singularity is naked) and the following restriction on α_{13} [44]

$$\alpha_{13} > -\frac{1}{2} \left(1 + \sqrt{1 - a_*^2}\right)^4. \quad (4)$$

Note that α_{13} enters the metric coefficients g_{tt} , $g_{t\phi}$, and $g_{\phi\phi}$. It thus affects the structure of the accretion disk, modifying the Keplerian gas motion and moving the ISCO radius. Qualitatively speaking, $\alpha_{13} > 0$ (< 0) increases (decreases) the strength of the gravitational force, so it moves the ISCO radius to higher (lower) values and this explains the strong correlation with the spin parameter in the plots shown in the Letter.

Data reduction and analysis

In our study, we analyzed 17 observations of the Proportional Counter Array (PCA). PCA was on board of

the *Rossi X-ray Timing Explorer (RXTE)*, which was launched in 1995 and decommissioned in 2012. PCA was designed to study far-away faint sources in the 2-60 keV energy range and consisted of 5 proportional counter units (PCUs), which comprised of Xenon layers to detect photons. We used the Heasoft version 6.25 to reduce the data and unprocessed data files were downloaded from the HEASARC website.

We used the pulse-height spectra of only PCU-2 because it is the best calibrated PCU and is the most operational one. ‘‘Standard 2’’ mode data were used for reduction. To derive the spectra, data from all the Xenon layers were combined for PCU-2. Background spectra were obtained by the latest ‘‘faint source’’ background model provided by the *RXTE* team and using the ftool PCABACKEST. The final spectra were then obtained by subtracting the background spectra from the total spectra. The response files were constructed and combined for each layer using the ftool PCARSP. We added a systematic error of 0.1% to all the PCA energy channels. Finally, the data were corrected for calibration using the python script PCACORR [45].

We only used data in the energy range 3-20 keV. Below 3 keV, calibration effects become dominant (see, e.g., Ref. [46]) and, in particular, the PCACORR correction is not valid in this regime. Above 20 keV, the background becomes dominant and the calibration is uncertain.

The best-fit values of observations 1-17 are reported in Tab. I.

No.	UT	$\alpha_{13} = 0$				α_{13} free				
		a_*	\dot{M}	f_{SC}	χ^2/dof	a_*	α_{13}	\dot{M}	f_{SC}	χ^2/dof
1	1996-06-09	$0.936^{+0.014}_{-0.015}$	$1.39^{+0.09}_{-0.08}$	$0.073^{+0.005}_{-0.005}$	38.08/42	$0.992^{+(\text{P})}_{-0.30}$	$0.29^{+0.05}_{-2.2}$	$1.34^{+0.15}_{-0.05}$	$0.073^{+0.005}_{-0.005}$	37.99/41
2	1996-08-01	$0.881^{+0.017}_{-0.018}$	$1.86^{+0.10}_{-0.10}$	$0.066^{+0.004}_{-0.004}$	23.13/42	$0.998_{-0.20}$	$0.59^{+0.10}_{-(\text{P})}$	$1.91^{+0.03}_{-0.23}$	$0.066^{+0.004}_{-0.004}$	23.08/41
3	1997-03-09	$0.943^{+0.009}_{-0.010}$	$1.47^{+0.07}_{-0.07}$	$0.050^{+0.004}_{-0.004}$	45.15/42	$0.998_{-0.27}$	$0.29^{+0.01}_{-1.7}$	$1.44^{+0.07}_{-0.10}$	$0.050^{+0.004}_{-0.004}$	45.02/41
4	1997-03-21	$0.948^{+0.007}_{-0.008}$	$1.48^{+0.05}_{-0.05}$	$0.046^{+0.003}_{-0.003}$	34.48/42	$0.998_{-0.28}$	$0.27^{+0.04}_{-2.0}$	$1.45^{+0.22}_{-0.02}$	$0.046^{+0.003}_{-0.003}$	34.24/41
5	1997-04-16	$0.921^{+0.009}_{-0.010}$	$1.64^{+0.06}_{-0.06}$	$0.056^{+0.003}_{-0.003}$	45.47/42	$0.998_{-0.24}$	$0.39^{+0.01}_{-1.6}$	$1.68^{+0.23}_{-0.16}$	$0.056^{+0.003}_{-0.003}$	45.07/41
6	1997-05-07	$0.938^{+0.008}_{-0.008}$	$1.55^{+0.06}_{-0.05}$	$0.053^{+0.003}_{-0.003}$	37.71/42	$0.993^{+(\text{P})}_{-0.48}$	$0.29^{+0.05}_{-2.2}$	$1.50^{+0.12}_{-0.04}$	$0.053^{+0.003}_{-0.003}$	37.51/41
7	1997-05-28	$0.964^{+0.012}_{-0.015}$	$1.31^{+0.11}_{-0.10}$	$0.058^{+0.007}_{-0.007}$	29.01/42	$0.995^{+(\text{P})}_{-0.34}$	$0.2^{+0.2}_{-3.1}$	$1.28^{+0.16}_{-0.18}$	$0.058^{+0.007}_{-0.009}$	28.92/41
8	1997-05-29	$0.938^{+0.016}_{-0.018}$	$1.42^{+0.11}_{-0.10}$	$0.049^{+0.006}_{-0.006}$	29.83/42	$0.996^{+(\text{P})}_{-0.40}$	$0.31^{+0.01}_{-4.4}$	$1.38^{+0.05}_{-0.05}$	$0.049^{+0.006}_{-0.005}$	29.76/41
9	1997-07-09	$0.917^{+0.017}_{-0.019}$	$1.57^{+0.11}_{-0.10}$	$0.046^{+0.005}_{-0.005}$	28.33/42	$0.274^{+0.003}_{-0.075}$	$-5^{+0.05}$	$1.014^{+0.005}_{-0.204}$	$0.049^{+0.003}_{-0.005}$	27.71/41
10	1997-08-20	$0.945^{+0.007}_{-0.008}$	$1.57^{+0.06}_{-0.06}$	$0.048^{+0.003}_{-0.003}$	34.47/42	$0.998_{-0.34}$	$0.29^{+0.05}_{-2.9}$	$1.53^{+0.04}_{-0.03}$	$0.048^{+0.003}_{-0.003}$	34.36/41
11*	1997-09-12	$0.906^{+0.010}_{-0.011}$	$1.76^{+0.06}_{-0.06}$	$0.048^{+0.003}_{-0.003}$	31.29/42	$0.2234^{+0.0424}_{-0.0014}$	$-5^{+0.05}$	$1.189^{+0.003}_{-0.085}$	$0.051^{+0.002}_{-0.003}$	29.62/41
12	1997-09-19	$0.964^{+0.008}_{-0.010}$	$1.31^{+0.07}_{-0.06}$	$0.063^{+0.004}_{-0.004}$	28.92/42	$0.994^{+(\text{P})}_{-0.19}$	$0.18^{+0.02}_{-0.72}$	$1.27^{+0.10}_{-0.13}$	$0.063^{+0.004}_{-0.004}$	28.77/41
13	1997-12-12	$0.925^{+0.010}_{-0.011}$	$1.65^{+0.07}_{-0.06}$	$0.042^{+0.003}_{-0.003}$	26.01/42	$0.93^{+(\text{P})}_{-0.82}$	$0.0^{+0.3}_{-(\text{P})}$	$1.65^{+0.08}_{-0.10}$	$0.042^{+0.003}_{-0.003}$	26.01/41
14	1998-03-12	$0.966^{+0.007}_{-0.007}$	$1.40^{+0.06}_{-0.04}$	$0.054^{+0.004}_{-0.004}$	30.37/42	$0.998_{-0.20}$	$0.19^{+0.21}_{-0.44}$	$1.39^{+0.05}_{-0.17}$	$0.054^{+0.004}_{-0.004}$	30.36/41
15	1998-05-06	$0.948^{+0.008}_{-0.009}$	$1.43^{+0.06}_{-0.06}$	$0.048^{+0.003}_{-0.003}$	28.01/42	$0.998_{-0.43}$	$0.27^{+0.05}_{-2.5}$	$1.40^{+0.12}_{-0.04}$	$0.048^{+0.003}_{-0.003}$	27.90/41
16*	1998-07-20	$0.936^{+0.009}_{-0.009}$	$1.52^{+0.06}_{-0.05}$	$0.042^{+0.003}_{-0.003}$	21.07/42	$0.55^{+0.28}_{-0.20}$	$-2.9^{+3.2}_{-(\text{P})}$	$1.19^{+0.15}_{-0.36}$	$0.044^{+0.003}_{-0.003}$	20.50/41
17*	2004-01-07	$0.935^{+0.018}_{-0.022}$	$1.45^{+0.13}_{-0.13}$	$0.046^{+0.005}_{-0.005}$	19.02/42	$0.54^{+0.26}_{-0.23}$	$-3.0^{+3.3}_{-(\text{P})}$	$1.1^{+0.3}_{-0.4}$	$0.048^{+0.005}_{-0.005}$	18.96/41

TABLE I. Best-fit values for observations 1-17 assuming the Kerr spacetime ($\alpha_{13} = 0$) and without such an assumption (α_{13} free). The reported uncertainties correspond to the 90% confidence level for one relevant parameter ($\Delta\chi^2 = 2.71$). Note that the maximum value of a_* allowed by the model is 0.998, while the minimum value of α_{13} is -5 . In several cases, the best fit is stuck at $a_* = 0.998$ or at $\alpha_{13} = -5$ and therefore we do not report the upper/lower uncertainty. (P) means that the 90% confidence level reaches the maximum/minimum value of the parameter. * marks the three “golden spectra”, which meet all the conditions for thermal dominant spectral data.